Multimodal Target Correction by Local Bone Registration: a PET/CT Evaluation.

Thiago Oliveira-Santos, Thilo Weitzel*, Bernd Klaeser, Thomas Krause, Lutz-Peter Nolte, Stefan Weber, Mauricio Reyes

***Abstract*—PET/CT guidance for percutaneous interventions allows biopsy of suspicious metabolically active bone lesions even when no morphological correlation is delineable in the CT images. Clinical use of PET/CT guidance with conventional step-by-step technique is time consuming and complicated especially in cases in which the target lesion is not shown in the CT image. Our recently developed multimodal instrument guidance system (IGS) for PET/CT improved this situation. Nevertheless, bone biopsies even with IGS have a trade-off between precision and intervention duration which is proportional to patient and personnel exposure to radiation. As image acquisition and reconstruction of PET may take up to 10 minutes, preferably only one time consuming combined PET/CT acquisition should be needed during an intervention. In case of required additional control images in order to check for possible patient movements/deformations, or to verify the final needle position in the target, only fast CT acquisitions should be performed. However, for precise instrument guidance accounting for patient movement and/or deformation without having a control PET image, it is essential to be able to transfer the position of the target as identified in the original PET/CT to a changed situation as shown in the control CT.**

Therefore, we present a pipeline for faster target-position correction by isolating and registering the bone of interest, as shown in the control CT, with the CT dataset of the original PET/CT acquisition. Challenges such as the masking of the bone of interest and registration robustness in the presence of the needle and its associated metal artifacts are also addressed in this work.

Our results confirmed the feasibility of clinically using this technique for target correction on PET/CT bone intervention, and motivated us to incorporate it as part of our IGS for multimodal intervention.

I. Introduction

Percutaneous image-guided bone needle interventions (i.e. biopsy, wire marking, radio frequency ablation, etc.) are widely used in medicine as a minimally invasive alternative to open surgical interventions. Such procedures are typically performed based on structural volumetric datasets, as for example, computed tomography (CT) and magnetic resonance imaging (MRI). However, medical imaging has changed fundamentally with the introduction of functional modalities such as Single Photon Emission Computer Tomography (SPECT) and Positron Emission Tomography (PET). Using combinations of structural and functional modalities (PET/CT, SPECT/CT), image understanding and diagnosis can be optimized [1], [2]. With these techniques even suspicious lesions without morphological correlation, i.e. not evident in structural datasets, can be identified and verified histologically, following biopsy [3].

In multimodal image interventions, the functional image provides information about the target (e.g. PET and SPECT) while the structural image provides information for instrument guidance (e.g. CT, MRI, etc.). Such procedures are usually performed using a step-by-step technique (similar to CT guided biopsy): Typically, the intervention is planned based on a single-bed co-registered PET/CT acquisition of the patient already positioned for intervention. The needle is then introduced in small steps alternated with repeated control CT acquisitions to ascertain its current position. After the trocar reaches the bone surface, the drilling towards the lesion starts. However, because of the increased time demand for regional PET acquisitions (2-4 min. for image acquisition plus 3-6 min. for image reconstruction), the step-wise control of the needle position is usually not performed as complete PET/CT, but as CT only acquisitions. These CT images may be co-displayed with the first acquired PET image, nevertheless it does not account for possible displacement of the lesion between the first PET/CT acquisition and the control CT scans. These displacements can occur because of patient movement, by the interaction between the needle and the bone when drilling [4], or by an involuntary rearrangement on the scanning table. Independent of their cause, these shifts may produce a significant target displacement in the co-displayed PET and control CT images during the intervention (according to clinical observations often 5-10mm), potentially leading to an erroneous needle placement. Consequently, the number of necessary punctures and CT image acquisitions increases which causes discomfort and unnecessary radiation exposure to the patient. This misalignment affects not only the standard PET/CT image guided procedure, but also a computer navigated guided intervention, which uses control CT images to update the current navigated scenario. In this type of system, the target position would be wrongly displayed and would therefore lead the physician to puncture in the wrong position. One way of correcting the target position without new PET acquisitions is by registering a control CT with the first

T. Oliveira-Santos, M. Reyes and L. P. Nolte are with the Institute for Surgical Technology & Biomechanics, Bern University, Bern, Switzerland

T. Weitzel (*corresponding author e-mail: thilo.weitzel@insel.ch), T. Oliveira-Santos, B. Klaeser and T. Krause are with Department of Nuclear Medicine, Inselspital Bern, 3010 Bern, Switzerland.

S. Weber is with the ARTORG Center for Biomedical Engineering Research, Bern University, Bern, Switzerland.

acquired CT.

Rigid and non-rigid image registration has been widely used for many years to address problems in the medical field, and has its basic concepts well described in [5]. In the bone PET/CT needle intervention scenario described above, the region of interest (ROI) is compounded of non-rigid and rigid structures (e.g. soft tissue and bones) that move independently to each other. In addition, control CT images contain the puncturing needle and metal artifacts that are not present in the first image and might affect the accuracy of standard registration algorithms, see fig 4 g and h.

In order to address these problems and be able to perform a real-time registration during clinical routine, this paper presents a registration pipeline capable of: extracting the bone of interest (BOI) without the needle and therefore turning the registration scenario into a rigid problem; registering a control CT with the first acquired CT; and finally, correcting the target location inside the bone. This paper also validates the method under different conditions (e.g. registration metrics, ROI sizes and initializations) using image data from a navigated PET/CT pilot study with pig cadavers. The implemented pipeline will be incorporated into our PET/CT image based instrument guidance system (IGS) [6] to allow for intra-procedural target position update without the need of a new PET acquisition.

II. Materials and Methods

In this section, detailed description of the implemented pipeline and the validation experiments are presented.

A. Implemented Pipeline

The registration pipeline presented here, was implemented with the open source Insight Toolkit (ITK) [7], and is mainly comprised of three parts (Fig. 1): reference mask generation, moving mask generation and registration. Its expected inputs are the first acquired CT, i.e. reference image, I_{ref}, a control CT, i.e. moving image, I_{mov}, and the target location in the reference image, P_{tpl}. The main difference between the proposed method and a standard registration (SR) approach is the addition of masks to restrict the registration to the BOI. A detailed description of the registration pipeline components is shown below:

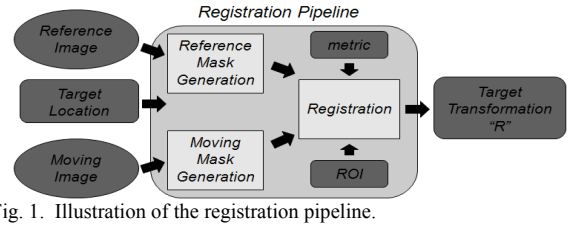

Fig. 1. Illustration of the registration pipeline.

1) Reference Mask Generation

In the reference image, one might find several structures not rigidly connected to the BOI that might affect the registration. To filter out all of these unwanted objects, a binary mask, I_{rfm}, is generated around the BOI. As a first step, a binary image is created by applying a lower threshold in the reference image to retain only the bone structures, Fig. 2b. Care is taken when choosing this value to ensure that different bones generate one binary blob per bone. In this study, an optimal threshold value covering most of the experiments and equal to the bone surface intensity was empirically found. Using P_{tpl} as a seed point, the closest blob of the threshold image is automatically selected as the BOI, Fig. 2c. This blob is then dilated (by an empirical radius of 6mm) to ensure the edges and the inner parts of the bone were included in the mask, Fig. 2d.

2) Moving Mask Generation

The presence of the puncturing needle and its associated metal artifacts make the moving image different from the reference image. To reduce this difference, these objects are filtered out through the application of a binary mask, I_{mvm}. As a first step, a binary image is generated with an upper and a lower threshold. Whereas the upper threshold is used to filter out needle and artifacts with high intensity values, the lower threshold is used to filter out shadow artifacts with low intensity values. In this study, the definition of these thresholds was performed assuming that the needle and its more prominent metal artifacts have intensity values higher than the bone values and lower than the soft tissue values, respectively. Therefore, the highest bone intensity value of a calibrated scanner was set as the upper threshold and the lowest soft tissue value was set as the lower threshold. To ensure the needle is completely masked out, an erosion filter with the empirical radius of 2mm (based on the needle thickness) is then applied to the mask.

3) Registration

The registration is the core part of the pipeline and utilizes the generated masks to constrain the registration metric to the BOI of the input images. Furthermore, it uses a regular step gradient descendent optimizer to calculate a 3D rigid transformation, R, that maps the reference image ROI (centered in the target location) to the moving image. Linear interpolation is used for re-sampling during registration.

B. Input Data Generation

The data from a navigated PET/CT biopsy pilot study using pig cadavers prepared with radioactive spots (lesions simulated by 1mm diameter cotton wool balls with ca. 0.5 MBq 18F solution placed inside bone) was used as input for the registration experiments. The image data was acquired with the animal cadaver lying down on the scanner table and in alternation with biopsy punctures. Two datasets (each containing co-registered PET/CT) were obtained per puncture: a planning dataset and a validation dataset. The planning dataset was acquired prior to each puncture. Its PET image was used here to define P_{tpl}, and its CT image was used as the reference image for the registration pipeline. The validation dataset was acquired right after each puncture with the needle in place. Its PET image was used to define the validation target location, P_{tva}, and its CT image was used as the moving image for the registration pipeline. The target positions were manually defined in every puncture using standard axial, sagittal, coronal viewers fusing PET

and CT images.

Image acquisition was accomplished with a Siemens Biograph 16 Hi-Rez with voxel size set to 1.37×1.37×1mm and 2.67×2.67×2mm, for CT and PET (intrinsic spatial resolution of 5 mm) respectively. Both image modalities share the same coordinate system. A bone biopsy set with a coaxial needle of 3.4 mm outer diameter (10 G) and 130 mm length was used.

C. Experiment Description

To validate the different components of the implemented pipeline, three experiments were performed: the *reference mask generation test* to assess the correctness of the BOI selection; the *pipeline parameters test* with the purpose of measuring the robustness against the metal artifacts not fully removed by masking, quantifying an optimal ROI size (feasible computational time with minimal information loss), and accessing the masking effect in the registration result; and finally, the *repeatability test* to measure the registration robustness against the initial deformation.

1) Reference Mask Generation Test

Besides the automatic masks (seed in P_{tpl}) generated while testing the registration pipeline, 40 additional masks were created with seed points manually selected in random locations of the BOI. Each additional mask was pixel-wise compared with its respective automatic mask to ensure the repeatability of the mask generation. A visual inspection, Fig 2d, was also performed to verify the BOI selection.

2) Pipeline Parameter Test

The registration pipeline was compared to the standard registration using four bone lesion datasets and different parameters, such as different ROI sizes (starting from 40×40×40mm and increasing 10mm in each axis up to 110×110×110mm) and different metrics (Mattes mutual information (MI) [8], [9] and normalized correlation (NC)). The experiment was performed as follow.

- For each puncture dataset, the I_{rfm} and I_{mvm} masks were generated for I_{ref}, and I_{mov} respectively.
- A set of registration transformations, R, were estimated with the registration pipeline (with I_{rfm} and I_{mvm} masks) and with the standard registration (without masks), using all different parameter combinations (ROI sizes and metrics).
- The accuracy evaluation was performed using the voxel-wise sum of absolute differences (SAD). However, in order to restrict the evaluation to the BOI and to generate a normalized value, only voxels inside the masks were considered in the sum. The SAD calculation was restricted by the masks even for the standard registration transformation that was estimated without masks. See the SAD formulation below:

$$I_{ad} = abs\left(I_{ref} - R \circ I_{mov}\right), \quad I_{cbm} = I_{rfm} - R \circ I_{mvm} \tag{1}$$

$$SAD = \left(\sum \left(I_{ad} \cap I_{cbm}\right)\right) / fnum\left(I_{cbm}\right) \tag{2}$$

Where, *abs* is the voxel-wise absolute value, ○ applies a transformation to an image, ∩ is the voxel-wise multiplication, *fnum* is the number of foreground voxels in the mask, and the mask images have background value 0 and foreground value 1.

3) Repeatability Test

To simulate distinct target movements, a total of 31 different initial transformations, T_{ini}, with translations of up to 11 millimeters and rotation of up to 11 degrees in each axis were applied to the moving image and to the P_{tva} of each puncture. The initial target distance, D_{ini}, was calculated ($|P_{tpl} - T_{ini}P_{tva}|$) for each different initial transformation. The registration R was then estimated for each $T_{ini} \circ I_{mov}$ using the parameters configuration (ROI size and metric) with a good tradeoff between computational time and registration accuracy (from the *pipeline parameter test*). Finally, the final target distance was calculated ($|P_{tpl} - RT_{ini}P_{tva}|$) per registration in order to assess the robustness against different target movements. Convergence was assumed for final target distance smaller than 1mm. The tests ran on a PC, Intel Core 2, 2.16GHz, 2G RAM.

III. Results

The reference mask of each puncture was repeatedly generated with the correctly BOI selection for most of the tested seeds, Fig. 2 illustrates one case. However, some seeds placed on rib parts bordering the spine wrongly selected a small portion of the rib which was not sufficient for registration.

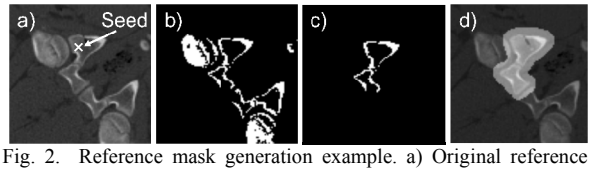

Fig. 2. Reference mask generation example. a) Original reference image. b) Binary bone outer surface threshold of image a). c) Seed point (cross) closest blob selected from image b). d) Resulting reference mask overlaid with image a).

The results of the *pipeline parameters test* are presented in Fig 3 and one example is illustrated in Fig. 4. The MI standard registration curve when compared to the MI and NC registration pipeline curves show the importance of the masks for cases like Puncture 1 and Puncture 3. One can see the standard registration accuracy decreasing with the increasing of the ROI size contrary to the registration pipeline curves. In these cases, bigger ROI sizes increased the presence of deformed regions in the registration. The standard registration NC peak in puncture 1 also shows the instability of the registration without mask when the ROI includes part of deformed regions. The effect of the needle and its metal artifacts can be verified through the NC standard registration curve in which the accuracy was affected for all four cases. The increase of the ROI size behavior is well illustrated by the registration pipeline curves in which an increase of accuracy is seen before reaching a more stable value. The registration pipeline with MI and NC did not show significant accuracy differences for the studied cases. However, the computation time of the used MI metric was more efficient than the NC, and therefore was chosen for further tests.

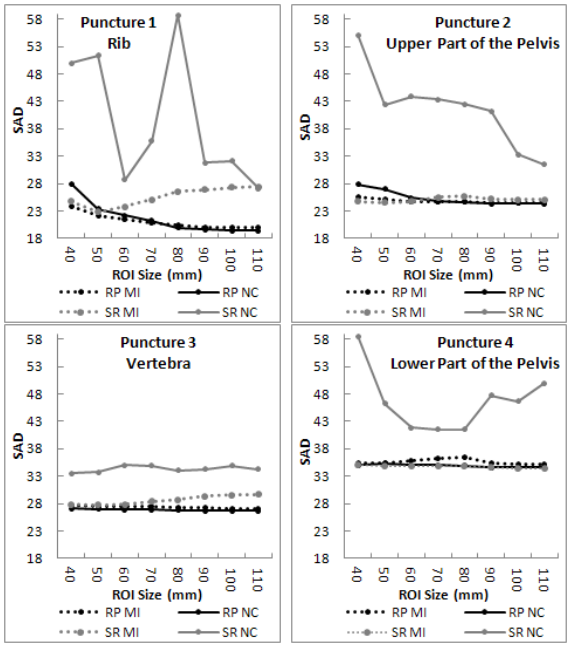

Fig. 3. Puncture graphs comparing the SAD behavior of the registration pipeline (RP) against standard registration (SR) using ROI sizes using MI and NC metrics.

The *repeatability test* results for MI metric and ROI size 90mm are presented in Table I. It shows the convergence percentage (CP) and registration time per D_{ini} range.

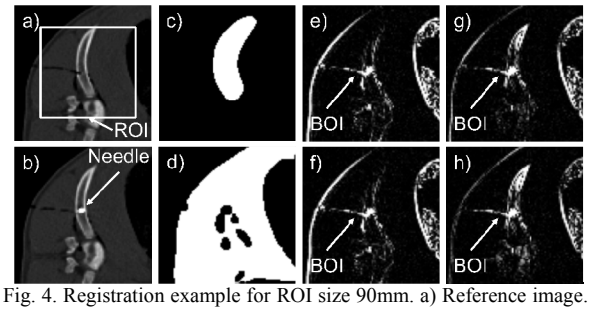

Fig. 4. Registration example for ROI size 90mm. a) Reference image. b) Moving image. c) Reference mask. d) Moving mask. e) Subtracted registration pipeline MI results. f) Subtracted registration pipeline NC results. g) Subtracted standard registration MI results. h) Subtracted standard registration NC results. Subtracted images are the absolute difference between reference and transformed moving image displayed with window/level equal to 200/100.

IV. Discussions and Conclusions

The reference mask correctly dissociated the surrounding structures of the BOI for most of the tested cases. However, a better segmentation would be desirable to cover all cases.

The *pipeline parameters test* demonstrated the importance of having a mask around the BOI even with the limited pig cadavers' deformation. The masking effect is expected to be even more evident with the greater deformation of real patients. The results also show that a small ROI size with the MI standard registration is enough for cases in which the ROI contains a BOI portion with enough information for registration and no deformed structures. The masking of the needle and its associated metal artifacts played an important role on NC metric and indicate a possible benefit for other linear metrics (e.g. sum of absolute differences). As the computational performance is an important factor, investigation with faster linear metrics should be performed.

TABLE I
Convergence Percentage per Initial Distance

Puncture	1		2		3		4	
D_{ini} up to:	CP	Time	CP	Time	CP	Time	CP	Time
10mm	71	210±62	100	170±57	100	232±73	100	79±45
20mm	5	248	88	144±47	87	196±41	35	155±156

Average time is given in seconds.

The *repeatability tests* showed the robustness against the initialization for most of the cases in the range up to 10mm which is sufficient for clinical routine. However, each bone presented a different D_{ini} range limit and would require a more detailed investigation for precise identification of each limit. Based on the tried transformations, puncture 1 (rib) could not stand big perpendicular shifts (8mm) or big angle deformations (11º), as it is a fine bone and its overlapped portion was compromised. More freedom was shown for punctures 2 and 3 that coped with D_{ini} of up to 19mm with only a couple of non converged cases. Puncture 4 converged stably for D_{ini} of up to 12mm. Computational time is still not ideal, however applicable to the studied scenario and open for optimizations not considered in this study.

The results obtained were encouraging and demonstrated the feasibility of the presented registration pipeline for correcting target positions during bone needle interventions based on multimodal images (e.g. PET/CT). This technique, allows for a more precise visualization of targets in a control CT image without having to acquire a new PET image which would also benefit IGS relying on such datasets.

References

[1] B. E. Hillner, B. A. Siegel, D Liu, A. F. Shields, I. F. Gareen, L Hanna, S. H. Stine, R. E. Coleman, "Impact of PET/CT and PET Alone on Expected Management of Patients With Cancer: Initial Results From the National Oncologic PET Registry," J. Clin. Oncol. 26, 2155-2161 (2008)

[2] E. Piperkova, B. Raphael, M. E. Altinyay et al., "Impact of PET/CT in Comparison with same dame contrast enhanced CT in Breast Cancer Management," Clin. Nucl. Med.; 32: 429 – 434 (2007)

[3] B. Klaeser, M. D. Mueller, R. A. Schmid, C. Guevara, T. Krause, J. Wiskirchen, "PET-CT-guided interventions in the management of FDG-positive lesions in patients suffering from solid malignancies: initial experiences," Eur Radiol.; 19:1780-5 (2009)

[4] N. Abolhassani, R. Patel, M. Moallem, "Needle insertion into soft tissue: A survey," Med. Eng. Phys. 29, 413-431 (2007)

[5] J. V. Hajnal, D. L. G. Hill, D. J. Hawkes, "Medical Image Registration. The Biomedical Engineering Series," CRC Press (2001)

[6] T. Oliveira-Santos, T. Weitzel, B. Klaeser, M. Reyes, S. Weber, "Introducing Computer-Assisted Surgery into combined PET/CT image based Biopsy," 9th Annual Meeting of CAOS-International Proceedings. 9, 308-311 (2009)

[7] L. Ibanez, W. Schroeder, L. Ng, J. Cates, T. I. S. Consortium, R. Hamming, "The ITK Software Guide," Kitware, Inc., Jan (2003)

[8] D. Mattes, D. R. Haynor, H. Vesselle, T. Lewellen and W. Eubank, "Nonrigid multimodality image registration", Medical Imaging 2001: Image Processing, pp. 1609-1620 (2001)

[9] D. Mattes, D. R. Haynor, H. Vesselle, T. Lewellen and W. Eubank, "PET-CT Image Registration in the Chest Using Free-form Deformations", IEEE Transactions in Medical Imaging. Vol.22, No.1, January. pp.120-128 (2003).